Nuclear Instruments and Methods in Physics Research A 593 (2008) 39–44

Contents lists available at ScienceDirect

Nuclear Instruments and Methods in Physics Research A

journal homepage: www.elsevier.com/locate/nima

Generation of ultra-short, high brightness electron beams for single-spike SASE FEL operation

J.B. Rosenzweig [a,*], D. Alesini [c], G. Andonian [a], M. Boscolo [c], M. Dunning [a], L. Faillace [b,c], M. Ferrario [c], A. Fukusawa [a], L. Giannessi [e], E. Hemsing [a], G. Marcus [a], A. Marinelli [b,c], P. Musumeci [a], B. O'Shea [a], L. Palumbo [b,c], C. Pellegrini [a], V. Petrillo [d], S. Reiche [a], C. Ronsivalle [e], B. Spataro [c], C. Vaccarezza [c]

[a] UCLA Department of Physics and Astronomy, 405 Hilgard Ave., Los Angeles, CA 90095, USA
[b] Universita degli Studi di Roma La Sapienza, Via Antonia Scarpa 14, Rome 00161, Italy
[c] INFN-LNF, via E. Fermi, 40– 00044 Frascati, Rome, Italy
[d] INFN-Milano, Via Celoria 16, 20133 Milan, Italy
[e] ENEA, via E. Fermi, 00044 Frascati, Rome, Italy

ARTICLE INFO

Available online 23 May 2008

ABSTRACT

In this paper, we study the production of low charge—in the 1 pC range—high brightness, ultra-short electron bunches, with a length shorter than 1 micromn, to produce sub-femtosecond pulses in an X-ray FEL. We show that the electron bunches have a brightness one or two orders of magnitude larger than the current photoinjectors run in their design regime. The ultra-short bunches can be used to drive a high gain SASE X-ray FEL with a small gain length, to produce femtosecond to attosecond X-ray pulses. This method to produce such short X-ray pulses has the advantage over other proposed methods in that it can be free from longer pulse duration background radiation. We also show, using nascent SPARX SASE FEL as an example, that the electron bunch thus produced can be shorter than the cooperation length of the X-ray FEL, leading to the production of a single spike, fully coherent, X-ray pulse. The proposed system for the production of ultra-short bunches uses the same injector hardware configuration of X-ray FELs like SPARX or the LCLS, operated with a different set of parameters, and does not require any new technical development in the injector and compressor systems.

1. Introduction

Recently there has been discussion of the idea [1] that one may employ an ultra-short electron beam—as short or shorter than the FEL cooperation length—and with very small charge, to drive short wavelength FELs [2–4]. Such beams may be extrapolated, based on known scaling, to have very high brightness, and thus be capable of driving short gain length with concomitant short cooperation length FELs. To produce single-spike operation [5], with the beam length equal to or smaller than a cooperation length, in an X-ray FEL, the beam should thus be made extremely short, in practice at or below the 1 fs level. In this regard, we have studied the creation, through initial velocity bunching [6,7] at low energy and subsequent chicane bunching [8], of ultra-low-charge ($\leqslant$1 pC) beams of sufficient quality to support strong FEL gain in the example of the SPARX FEL [9] run at 3 nm. Extension of this scheme to the LCLS [2] is also discussed in a companion paper in these proceedings [10].

In both cases we find that these beams can drive the FEL in single spike or near single-spike mode; one may therefore obtain SASE sources of coherent X-rays that have pulse lengths in the 1 fs regime, and with near transform limited performance. Thus full transverse and nearly full longitudinal coherence are possible. Even neglecting their enhanced coherence properties, it is interesting to compare this method of producing sub-femtosecond bunches with other methods proposed in the literature, all of which are based on employing a long electron bunch. These schemes then use some form of beam manipulation to select a small fraction of the electrons for lasing. However, the remaining beam electrons produce a long background signal that is absent in the method proposed here, with clear advantages for the experimental use of the X-rays. The proposed method of obtaining these short pulses is, further, accessible through changes only in running conditions of existing FELs, or those under construction, with only nominal changes in running conditions and experimental infrastructure.

This paper is organized as follows: we first quantitatively review the beam requirements that such a novel operating regime imply; we then work backwards through the machine to give insight into the constraints of ultra-short pulse operation.

* Corresponding author. Tel.: +1 310 206 4541; fax: +1 310 206 5251.
E-mail address: rosen@physics.ucla.edu (J.B. Rosenzweig).

0168-9002/$ - see front matter © 2008 Elsevier B.V. All rights reserved.
doi:10.1016/j.nima.2008.04.083

This inquiry proceeds first through the chicane compressor. We discuss the requirements on the beam before chicane compression, given a certain final expected bunch length and energy spread. We then go through the exercise of generating such beams, through a combination of launching ultra-short, very low charge beams in the photoinjector, employing scaling laws to quickly determine the operating point of the device, and its expected performance. We then use a velocity bunching scheme to arrive at the needed beam parameters. The process of electron beam creation and velocity bunching is simulated with PARMELA, while the final compression is modeled using ELEGANT. Finally, we verify the performance of the FEL systems using GENESIS.

From the viewpoint of the beam, we find a wide variety of advantages in operation with ultra-low charge. First, of course, is that ultra-short beams are possible, along with low emittances—in other words, high brightness electron beams naturally result from the photoinjector [11]. In addition, there are a number of problems that are almost entirely mitigated in this scenario, having to do with the beam's interaction with its environment. These issues, which include coherent synchrotron radiation (CSR) [12,13] in the chicane compressor as well as surface roughness and resistive wall wakes in the undulator vacuum wall [14–16], will be discussed in a subsequent work. This follow-on work will also discuss the challenges and opportunities for experimentally realizing operation of the beam in this environment.

2. Requirements of the free-electron laser

At short wavelengths, we may assume that the FEL performance is approximately described by the 1D theory [17]. In this case, we begin with the 1D dimensionless gain parameter, given by

$$\rho_{1D} = \left[\frac{JJ(K_{rms})K_{rms}k_p}{4k_u}\right]^{2/3} \tag{1}$$

where $k_u = 2\pi/\lambda_u$ is the undulator wave number; $K_{rms} = e\sqrt{\langle B_u^2\rangle}/k_u m_e c$ is the rms undulator parameter; $JJ(K_{rms})$ is the coupling factor, which is slightly below unity in a planar undulator; and $k_p = \sqrt{4\pi r_e n_b/\gamma^3} = \sigma_x^{-1}\sqrt{2I_b/I_0\gamma^3}$ (with the Alfven current $I_0 = ec/r_e \approx 17\,\mathrm{kA}$) is the relativistic beam plasma frequency.

The one-dimensional exponential gain length is given by

$$L_{g,1D} = \frac{\lambda_u}{4\pi\sqrt{3}\rho_{1D}} \tag{2}$$

and the cooperation length, defined as the slippage distance over one gain length, is

$$L_{c,1D} = \frac{\lambda_r}{4\pi\sqrt{3}\rho_{1D}}, \tag{3}$$

as the radiation overtakes the beam electrons by one radiation wavelength

$$\lambda_r \cong \frac{\lambda_u}{2\gamma^2}[1 + K_{rms}^2] \tag{4}$$

per undulator period. For single-spike operation, the bunch length should approximately obey

$$\sigma_{b,SS} < 2\pi L_{c,1D} = \frac{\lambda_r}{2\sqrt{3}\rho_{1D}} \tag{5}$$

In the case of SPARX design parameters [9], for operation at $\lambda_r = 3\,\mathrm{nm}$, $\rho_{1D} = 1.8\times10^{-3}$, and a single-spike bunch length is estimated as $\sigma_{b,SS} = 0.48\,\mu\mathrm{m}$ (1.6 fs).

Note that the ρ-parameter is weakly dependent on the quantity that we intend to change in this study, the beam density n_b, as $\rho_{1D} \propto (n_b)^{1/3} \propto (I_b/\varepsilon_n)^{1/3}$. In any case we shall see that for very low charges, it is possible to obtain operating conditions in which the current decreases in comparison to standard operation, while the normalized emittance ε_n decreases more dramatically. Thus the ρ-parameter increases and the gain length decreases and one may operate a given saturating (in standard design case) FEL deeper in saturation.

3. Scaling of beam compression

The compression processes that we employ in creating the final beams are of two types, velocity bunching at low (~5 MeV) energy and chicane bunching (usually two stages) at high (>500 MeV) energy. Because longitudinal space–charge dominates the beam dynamics in velocity bunching (just as the transverse space–charge dominates the beam size in emittance compensation dynamics, see Section 4), one may deduce the scaling for the bunch length after velocity bunching, in a given design scenario, to be $\sigma_\zeta \propto Q^{1/3}$. On the other hand, for chicane bunching at high energy, in the limit of low charge that we are examining, collective effects are strongly diminished compared to standard cases. In this case, the derivation of scaling laws concerning compression is also straightforward.

If we consider for the moment the limit of vanishing "slice" energy spread, the initial momentum distribution as a single-valued function of longitudinal coordinate ζ before the first chicane compressor is approximately [18]

$$\begin{aligned} p_z(\zeta) &\cong p_{max}\sin(k_{RF}\zeta) \\ &\cong p_0\left[1 - \cot(\phi_0)k_{RF}\delta\zeta - \frac{1}{2}(k_{RF}\delta\zeta)^2\right] \end{aligned} \tag{6}$$

Here $k_{RF} = 2\pi/\lambda_{RF}$ is the RF wave number, ϕ_0 is the reference particle's RF phase, $\delta\zeta = \zeta - \phi_0/k_{RF}$, and we have taken for a linac accelerating section of length L_{acc} the maximum achievable momentum to be approximately $p_{max}c \cong qE_0L_{acc}$. The first momentum deviation term on the right-hand side of Eq. (6) is the linear chirp, which can be partly or completely removed by the action of the chicane.

We must also add a "thermal" or uncorrelated momentum spread $\sigma_{\delta p,th} = \sqrt{\delta p_{th}^2}/p_0$, which is found from simulations, to the correlated momentum given in Eq. (6). This term, which originates in the strong space–charge-induced distortions arising during velocity bunching, dominates the final bunch length for ultra-short beams. To describe the situation before the chicane, it is useful to employ the second moments of the distribution:

$$\langle\delta\zeta^2\rangle = \sigma_\zeta^2 \tag{7}$$

$$\frac{\langle\delta p^2\rangle}{p_0^2} = \frac{(k_{RF}\sigma_\zeta)^4}{2} + \cot^2(\phi_0)(k_{RF}\sigma_\zeta)^2 + \sigma_{\delta p,th}^2 \tag{8}$$

$$\frac{\langle\delta\zeta\delta p\rangle}{p_0} = -\sigma_\zeta\cot(\phi_0)(k_z\sigma_\zeta) \tag{9}$$

The chicane is employed to partially or fully remove the correlation between the deviation in longitudinal position and momentum error $\delta p = p - p_0$.

Usually, one is restricted to considering partial compression, so that a linear chirp remains, which can be taken out using post-acceleration, with phase chosen back of crest. In the case of an ultra-short initial beam, where $\sigma_\phi = k_{RF}\sigma_\zeta \ll 1$, one may completely compress, to obtain the shortest possible beam and highest current. This compression may be performed at the final FEL energy, or as is more typical, at a lower energy, in which case the

post-acceleration diminishes the relative momentum spread by the ratio of the chicane-to-final momenta.

With the assumption of full (and significant, meaning $\delta p_{\rm th}/p_0 \ll k_{\rm RF}\sigma_\zeta \cot\phi_0$) compression, the chicane must have a longitudinal dispersion of [18]

$$R_{56} = \frac{k_{\rm RF}\sigma_\zeta^2 \cot(\phi_0)}{1/2(k_{\rm RF}\sigma_\zeta)^4 + (k_{\rm RF}\sigma_\zeta)^2\cot^2(\phi_0) + \sigma_{\delta p,\rm th}^2}$$
$$\Rightarrow \quad k_{\rm RF}\sigma_\zeta \ll 1 \qquad \frac{1}{k_{\rm RF}\cot(\phi_0)} = \frac{\lambda_{\rm RF}\tan(\phi_0)}{2\pi} \qquad (10)$$
$$\delta p_{\rm th}/p_0 \ll k_{\rm RF}\sigma_\zeta \cot\phi_0$$

Under this condition the compression (final-to-initial bunch length) ratio is given by

$$\frac{\sigma_\zeta^*}{\sigma_\zeta} \cong \frac{\sigma_{\delta p,\rm th}}{\sqrt{\sigma_{\delta p,\rm th}^2 + (k_{\rm RF}\sigma_\zeta)^2\cot(\phi_0)}} \qquad (11)$$

Note that in the limit of an initially long beam, one has the scaling $\sigma_\zeta^* \propto k_{\rm RF}\sigma_\zeta^2$; an already short beam can be made much shorter. In the limit we consider here, however, the bunch length is limited by the relative thermal momentum spread $\sigma_{\delta p,\ \rm th}$. This quantity is set by the process of velocity bunching, in which longitudinal space–charge gives thermal-like distortions to the phase space. In the case of the simulations we have performed, discussed below, the rms uncorrelated energy spread after velocity bunching is $\sim 35[Q(pC)]^{1/3}$ keV, a value which is then invariant during subsequent acceleration. We note in this regard that compression at the highest energy thus produces the shortest beams.

At this point, a numerical example, that of the SPARX FEL operated at 2 GeV, serves to illustrate the demands that single-spike operation make on the bunch length upstream of the chicane. For the single-spike bunch length as calculated above, we should have an rms bunch length at the FEL of $\sigma_\zeta^* \cong 480$ nm. Such a bunch length would be possible according to Eq. (11), compressing at full energy, and choosing $\phi_0 = 67^\circ$ in S-band RF (2856 MHz), with a pre-chicane bunch length of $\sigma_\zeta = 9\,\mu$m, implying a factor of 20 in compression. With these conditions, we must examine the rms momentum spread in the beam, to ensure consistency with the condition

$$\sigma_{\delta p} \cong \cot(\phi_0)(k_z\sigma_\zeta) \ll \rho_{1\rm D} \qquad (12)$$

With S-band RF, we have $\sigma_{\delta p} \cong 2.1\times10^{-4}$ and $\rho_{1\rm D} > 1.8\times10^{-3}$ (this is the nominal SPARX design value, which may be enhanced in higher brightness operation) so Eq. (12) is satisfied.

We shall see below that the energy spread is not significantly enhanced during the chicane bunching due to CSR. In order to explain this, we can use the simple model recently given by Bosch [19] for estimating the maximum energy loss per electron, which occurs near the beam longitudinal center. For a maximum current of $I_{\rm max}$, the rms energy loss is approximately

$$\sigma_{\rm E} = \frac{Z_0 I_{\rm max}}{4\pi}\ln\left[\frac{\sigma_z\gamma^3}{R\sqrt{2\pi}}\right] \qquad (13)$$

Here $Z_0 = 377\,\Omega$ is the impedance of free space, and R is the bend radius of curvature in the chicane magnets. In order to achieve the compression, the correct $R_{56} \cong \frac{4}{3}R\theta_{\rm b}^3$ [17] factor mush be chosen. Taking, consistent with previous SPARX designs, a magnet bend angle of $\theta_{\rm b} = 25$ mrad (1.43°), we have $R = 830$ m. With these parameters, we obtain $\sigma_{\delta p} \cong \sigma_{\rm E}/E \cong 10^{-5}$. This is much smaller than the pre-existing momentum spread, and thus is not inherently dangerous. One must, however, check that the radiative energy loss due to CSR inside of the chicane does not cause significant emittance growth. We discuss this issue in Section 4.

In the case of velocity bunching at low energy, the minimum compression ratio is not subject to the considerations above, as it is limited by space–charge effects. Through simulations, we have found that this ratio is, for short, longitudinal space–charge dominated beams (i.e. not subject to RF curvature limits), approximately constant at 0.1. This constant ratio is expected, as the launch value of the (laser) rms length must also scale as $\sigma_0 \propto Q^{1/3}$, as is discussed in the following section. Thus the beam launched from the gun should have a pulse length of $\sigma_0 \cong 10\sigma_\zeta \cong 90$ μm (0.3 ps).

4. Photoinjector scaling

With the choice of bunch length dictated by the physics of the FEL and the two downstream compression processes, we can directly deduce the correct scaled beam charge Q that should be used to obtain the desired pulse length σ_0. We consider standard (LCLS-like) operation of the RF gun and emittance compensation solenoid. In order to scale to shorter pulse length, one must keep the beam density (and thus the beam plasma frequency $k_{\rm p} \propto n_{\rm b}^{1/2}$, which dictates the correct emittance compensation dynamics) constant [8]. In the standard case (Ferrario operating point [20]), we have $Q = 1$ nC and $\sigma_0 = 0.87$ mm. In order to scale the beam density and aspect ratio correctly, we have the condition on the beam sizes, in all dimensions, that $\sigma_i \propto Q^{1/3}$. Thus to obtain a bunch length one order of magnitude smaller, we should lower Q by a factor of 1000, from 1 nC to 1 pC.

One can predict the behavior of emittance in this case, as charge scaling in the Ferrario operating point has been studied extensively [21]. The contributions to the emittance scale as follows:

$$\varepsilon_{x,\rm sc} \propto k_{\rm p}^2\sigma_x^2 \propto Q^{2/3} \ \text{(space charge)} \qquad (14)$$

$$\varepsilon_{x,\rm RF} \propto \sigma_z^2\sigma_x^2 \propto Q^{4/3}, \ \text{(RF/chromatic effects)} \qquad (15)$$

$$\varepsilon_{x,\rm th} \propto T_c^{1/2}\sigma_x \propto Q^{1/3} \ \text{(thermal emittance)} \qquad (16)$$

At very low charge, the "thermal" emittance due to the inherent spread in photoelectron transverse momentum indicated by a temperature $T_{\rm c}$ must dominate. To illustrate this point, we can write the emittance for this family of designs as follows:

$$\varepsilon_{\rm n}(\text{mm-mrad}) = \sqrt{a_1 Q^{2/3} + a_2 Q^{4/3} + a_3 Q^{8/3}} \qquad (17)$$

where Q is in nC and from simulation studies we have $a_1 = 0.111$, $a_2 = 0.18$, $a_3 = 0.18$. With $Q = 1$ pC, one has a thermally dominated emittance of 0.033 mm-mrad.

If there were no emittance growth in this scheme, one would have a final beam current of 250 A, and thus a brightness of $B = 2I/\varepsilon_{\rm n}^2 = 4.5\times10^{17}$ A/m^2, which is *two orders of magnitude higher* than the value indicated for the nominal design. Indeed, we will find that there is a factor of two emittance growth due to space–charge during velocity bunching, but we will still obtain a beam with much higher brightness using this scheme.

One may estimate the emittance growth due to CSR energy loss using a simple calculation based on Bosch's heuristic model. Assuming the energy loss mainly arises (due to coherent edge radiation) at the magnet exit/entrance in bends 3/4, the minimized emittance growth due to uncancelled dispersion after the chicane may be estimated, in the SPARX case, as

$$\Delta\varepsilon_{\rm n} \cong \gamma\sigma_{\delta p}^2\frac{R\theta_{\rm b}^3}{\sqrt{2}} \cong 6\times10^{-9}\ \text{m-rad} \qquad (18)$$

Note that this is an order of magnitude smaller than the emittance obtained after velocity bunching, thus explaining the

lack of emittance growth observed in the simulations discussed in the next section.

5. Beam simulations

We consider here the case of the SPARX S-band injectors and linacs. The injector and velocity bunching sections are simulated with UCLA PARMELA [22], while the downstream linac and compression simulations are performed with ELEGANT [23]. In the SPARX case the chicane compression is assumed to be performed at full energy, as allowed by the momentum spread condition.

The injector parameters are summarized in Table 1. The beam dimensions are scaled simply from the standard Ferrario operating point by dividing by 10, yielding a charge diminished by a factor of 1000. The velocity bunching is effective at producing a bunch an order of magnitude shorter than the laser pulse. The performance of the combined emittance compensation/velocity bunching processes is described in Figs. 1 and 2, which display the evolution of the beam bunch length and emittance. It can be seen that velocity bunching is employed at the cost of some additional transverse (above thermal) emittance and longitudinal momentum spread, as discussed above. The parameters resulting from this set of simulations are quite sufficient for driving an FEL.

Table 1
Parameters for ultra-low charge UCLA PARMELA simulations with emittance compensation and velocity bunching

Charge	1 pC (6.2E6 electrons)
Laser pulse length (rms)	290 fs
Gun max on-axis E	110 MV/m
Ave. traveling wave E_z	13.5 MV/m
Laser beam radius (full)	100 μm
Thermal emittance $\varepsilon_{x,\,th}$	0.033 mm-mrad
ε_n after velocity bunching	0.062 mm-mrad
Final bunch length (rms)	9 μm (28 fs)
Energy after velocity bunching	17.9 MeV
Final $\sigma_{\delta p}/p$	0.31%

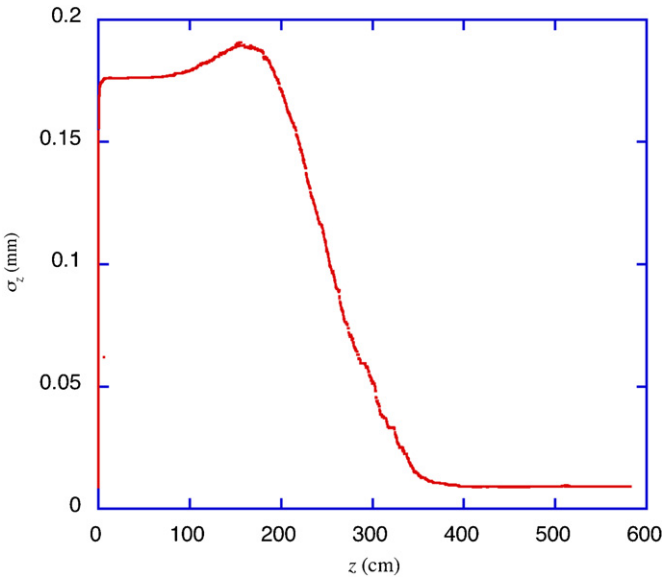

Fig. 1. Evolution of beam longitudinal rms size during emittance compensation, velocity bunching.

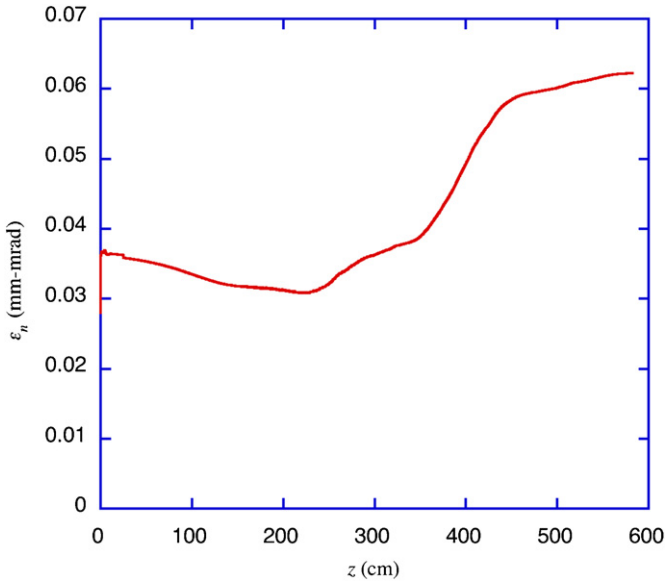

Fig. 2. Evolution of beam rms emittance during emittance compensation and velocity bunching.

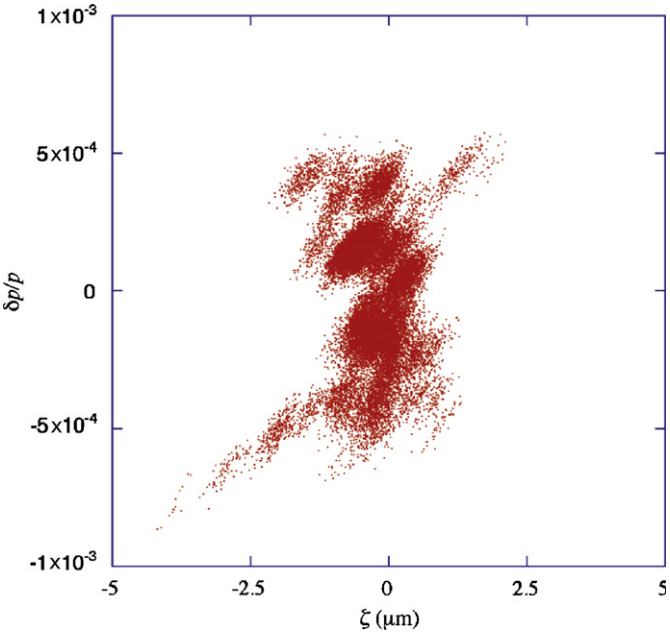

Fig. 3. Longitudinal phase space at SPARX undulator entrance.

After the low energy section, we present the compression relevant to the SPARX FEL run at an energy of 2 GeV. The longitudinal phase spaces at final energies are displayed in Fig. 3. Note that we are compressing fully, which implies both maximum current and momentum spread. The rms relative momentum spread within the high-current beam (profile shown in Fig. 4) core is $\sigma_{\delta p} = 2.4 \times 10^{-4}$. The rms bunch length in the SPARX example is $\sigma_z = 4.67$ nm (1.56 fs). Thus we are able to approach the femtosecond frontier in electron beam creation using this method.

A key advantage of ultra-low beam charge operation is that the beam emittance does not notably degrade due to collective effects during compression. Thus, with the values of the peak current

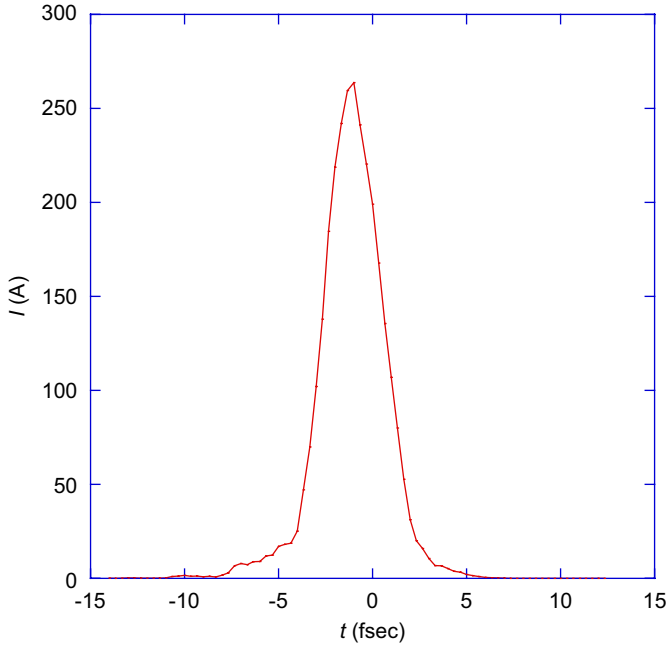

Fig. 4. Beam current profile at the entrance of the SPARX undulator.

obtained and a normalized emittance of $\varepsilon_n = 6.2 \times 10^{-8}$ mrad, the beam brightness is greatly increased—it is $B = 1.35 \times 10^{17}$ A/m^2 (by over two orders of magnitude) in the SPARX example, only slightly degraded from our estimate above due to emittance growth during velocity bunching.

We note that because full compression has been employed twice in the preparation of the ultra-high brightness fsec beam described above. As such, the scheme we have used is less sensitive to timing jitter in the RF and laser systems than those that depend on partial compression (e.g. standard scenarios for the LCLS).

To illustrate this, we discuss the most important likely jitter source, errors in injection timing of the laser onto the photocathode. We take a representative laser-RF wave jitter of 0.5 ps. In this case the velocity bunching produces a beam with ~0.6% different peak current, because the compression's "longitudinal waist" is space–charge dominated. In addition, the longitudinal focusing serves to partially (not completely, again due to space–charge [24]) remove the initial timing jitter; only 190 fs of jitter with respect to the RF wave remains. We note that the transverse phase space is little affected by this jitter. Injecting the beam with slightly modified initial phase space and 0.19 ps timing error into the downstream linac and compressor produces a final compressed beam with ~1.4% less peak current (and commensurate negligible bunch lengthening) as compared to Fig. 4.

6. Free-electron laser simulations

We complete the experimental scenario for SPARX by simulating the FEL performance. The parameters of the simulations, performed with Genesis 1.3 [25], are given in Table 2. We note that the undulator and electron beam focusing parameters are kept the same as in reference design, despite the fact that they may no longer be optimum with such high brightness beams. In short, one might focus harder, as with smaller emittances, the maximum rms angles in the beam ($\sigma_\theta = \sqrt{\varepsilon_n/\beta\gamma}$) tolerated by the FEL are not reached without much stronger focusing (i.e. smaller β). On the other hand, the present exercise serves to show the ease in which the FEL designs may be adapted to employing ultra-low charge, ultra-high brightness beams. Other considerations also enter into the choice of focusing, such as diffraction.

Table 2
Parameters for Genesis simulation of SPARX FEL with ultra-short beam

Undulator wavelength λ_u	2.8 cm
Undulator strength K_{rms}	1.516
Resonant wavelength λ_r	3 nm
Focusing β-function	12.5 m
Gain parameter ρ_{1D}	2.3×10^{-3}

The results of the Genesis simulations are shown in Fig. 5. The most compelling aspect of the FEL as simulated, displayed in Fig. 5(b), is that one indeed has achieved single-spike performance, with a radiation pulse having 0.36 micron (1.2 fs) rms length. Further, this pulse has, at its narrowest, a wavelength spectrum (Fig. 5(c)) that gives and time-bandwidth product only a factor of 1.2 above the Fourier transform limit.

One may also see that the transverse beam size in the undulator, $\sigma_x = \sqrt{\beta\varepsilon_n/\gamma} = 14\,\mu$m, is such that diffraction even plays a role in the gain process, as the "Rayleigh range" $Z_R 4\pi\sigma_x^2/\lambda_r$ associated with the beam size (assuming a radiation mode size equal to the electron beam size) is only 83 cm. Because the assumed Z_R is less than the actual gain length, the radiation mode is larger than the electron beam. This further implies that, in the SPARX case, stronger focusing would not produce significantly enhanced performance; in effect, the gain is only sensitive to the beam current, and not current density in this regime.

7. Conclusions and future work

As can be seen from the discussion given above, this scheme works very well, single-spike operation predicted in the SPARX FEL. It should be emphasized that in order to obtain the ultra-short, ultra-small Q beams using the nominal bunching mechanisms, one need not use any significant additional hardware in both the SPARXand the LCLS case. Extension of low-charge, ultra-short beam philosophy to the LCLS, in which sub-fsec performance is examined, is discussed in Ref. [10].

Single-spike operation should give tremendous advantages not only in pushing the frontier of X-ray FEL pulses to sub-fsec time resolution, the level of *atomic electron* motion. To reach this threshold, in comparison to other schemes, such as the slit-spoiler method [26], chirped pulses [27], enhanced SASE [28], the ultra-low charge option has decided advantages. First, none of these competing schemes mitigate the collective effects in the linac and compression systems in the way foreseen for the ultra-low chare scheme. In addition, the other schemes do not produce a pedestal-free X-ray pulse. This may be a critical advantage in X-ray experimentation at free-electron laser facilities.

There are also clearly challenges in using these types of pulses in the context of existing or modified injectors and accelerators. First, we note that the total dark current obtained in high field operation of S-band photoinjectors tends to be on the 1 nC level. Thus integrating detectors such as screens (particularly just after the gun) will have some background issues. One may "clean up" the dark current using two anti-phased RF deflectors, separated by an odd multiple of π betatron phase advance, with collimators placed in between.

Just as interesting is the question of beam diagnostic resolution; one must be able to measure very small emittances and

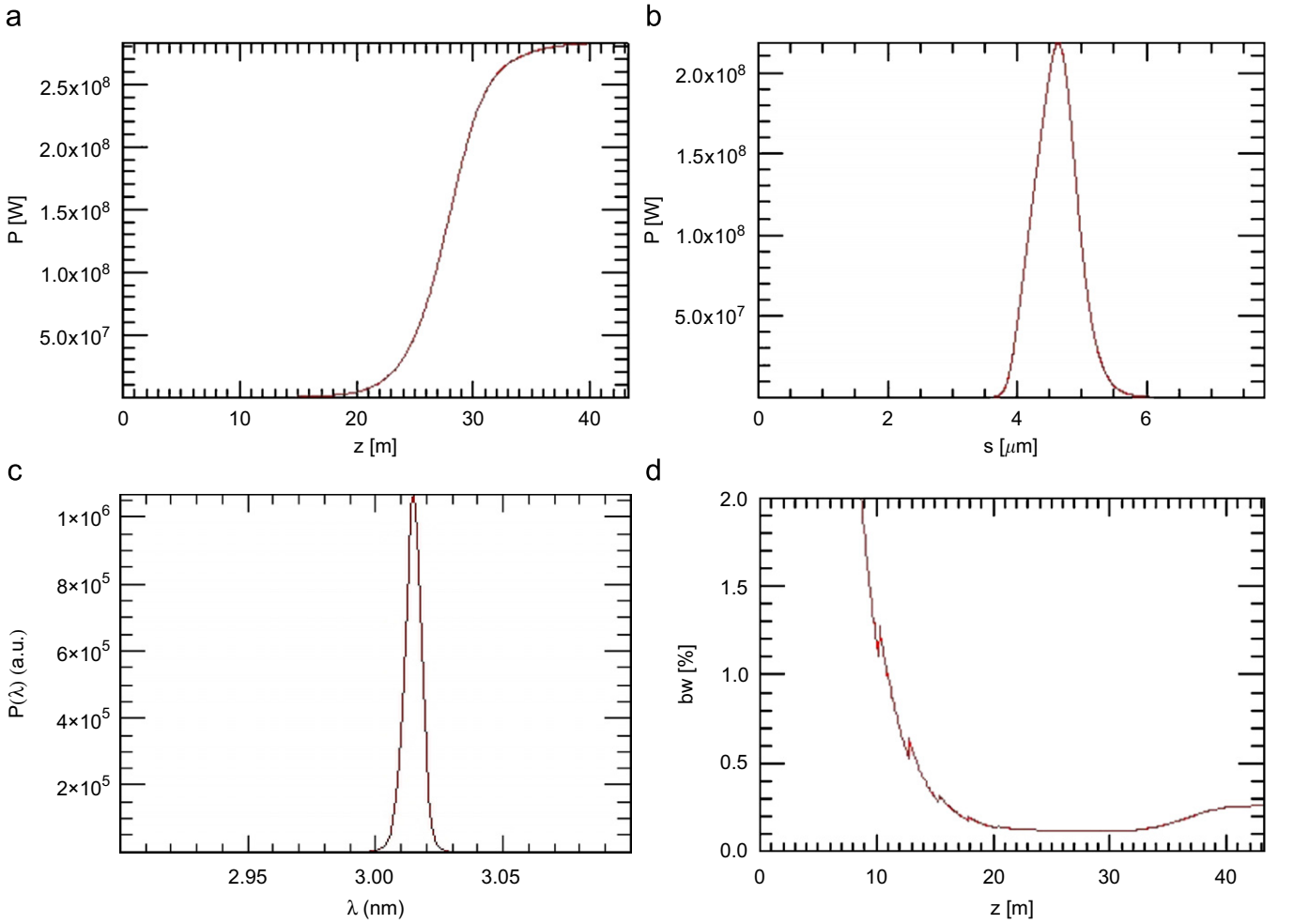

Fig. 5. Results from Genesis simulations, with input particles taken from the output of beam simulations, of the SPARX FEL. (a) Power vs. distance along the undulator z, (b) power as a function of s at undulator exit (c) power spectrum at undulator exit, (d) relative bandwidth as a function of z.

extremely short bunch lengths. We note in this regard that beam after velocity bunching will emit coherently (in, e.g., diffraction radiation) in the far IR. An even more compelling scenario is obtained for these beams after final compression, as they would emit (in, e.g., CER/CSR from the final chicane dipole) coherent visible to IR light. The expected signal, despite the low charge, is quite robust.

References

[1] M. Ferrario, et al., private communication;
C. Pellegrini, private communication.
[2] R. Bonifacio, C. Pellegrini, L. Narducci, Opt. Commun. 50 (1984) 373.
[3] Linac Coherent Light Source Conceptual Design Report, SLAC-R-593, SLAC, 2002.
[4] TESLA Technical Design Report, TESLA FEL 2002-09, DESY, 2002.
[5] R. Bonifacio, L.D. Salvo, P. Pierini, N. Piovella, C. Pellegrini, Phys. Rev. Lett. 73 (1994) 70.
[6] L. Serafini, M. Ferrario, in: S. Chattopadhyay, (ed.), Physics of, and Science with, the X-ray Free-Electron Laser, AIP Conf. Proc. No. 581 AIP, New York, 2001.
[7] S.G. Anderson, P. Musumeci, J.B. Rosenzweig, W.J. Brown, R.J. England, M. Ferrario, J.S. Jacob, M.C. Thompson, G. Travish, A.M. Tremaine, R. Yoder, Phys. Rev. ST-Accel. Beams 8 (2005) 014401.
[8] J.B. Rosenzweig, N. Barov, E. Colby, IEEE Trans. Plasma Sci. 24 (1996) 409.
[9] C. Vaccarezza, et al., Proc. European Particle Accelerator Conf. 2006, 107 (JACOW, 2006).
[10] S. Reiche, et al., these proceedings.
[11] J.B. Rosenzweig and E. Colby, Advanced Accelerator Concepts p. 724 (AIP Conf. Proc. 335, 1995).
[12] S. Heifets, G. Stupakov, S. Krinsky, Phys. Rev. ST Accel. Beams 5 (2002) 064401.
[13] S. Reiche, J.B. Rosenzweig, Phys. Rev. ST Accel. Beams 6 (2003) 040702.
[14] A. Mostacci, et al., in: J. Rosenzweig, Ed. L. Serafini and G. Travish, (ed.), The Physics and Applications of High Brightness Electron Beams, (World Scientific, 2003).
[15] G. Stupakov, et al., Phys. Rev. ST Accel. Beams 2 (1999) 060701.
[16] F. Zhou, et al., Phys. Rev. Lett. 89 (2002) 174801.
[17] Zhirong Huang, Kwang-je Kim, Phys. Rev. ST Accel. Beams 10 (2007) 034801.
[18] James Rosenzweig, Fundamentals of Beam Physics, Oxford University Press, 2003.
[19] R.A. Bosch, Phys. Rev. ST Accel. Beams 10 (2007) 050701.
[20] M. Ferrario, J.E. Clendenin, D.T. Palmer, J.Rosenzweig and L. Serafini, in: J. Rosenzweig and L. Serafini, (eds.), The Physics of High Brightness Beams, 534, 2000.
[21] M. Ferrario, W.D. Moeller, J.B. Rosenzweig, J. Sekutowicz, G. Travish, Nucl. Instrum. Methods A 57 (2006) 98.
[22] E. Colby, UCLA PhD Thesis, FERMILAB-THESIS-1997-03 (FNAL, 1997).
[23] M. Borland, 〈http://www.aps.anl.gov/asd/oag/oaghome.shtml〉.
[24] M. C. Thompson and J. B. Rosenzweig, Proc. 9th Advanced Accel. Concepts Workshop 374 (AIP Conf. Proc. 569, 2001).
[25] S. Reiche, Nucl. Instrum. Methods A 429 (1999) 243.
[26] P. Emma, et al., Phys. Rev. Lett. 92 (2004) 074801.
[27] Z. Huang, S. Krinsky, Nucl. Instrum. Methods A 528 (2004) 28.
[28] A. Zholents, Phys. Rev. ST Accel. Beams 8 (2007) 040701.